The Influence of Buoyancy Flux from Estuaries on Continental Shelf Circulation

ANDREW J. WEAVER* AND WILLIAM W. HSIEH

Department of Oceanography, University of British Columbia, Vancouver, BC Canada, V6T 1W5

(Manuscript received 24 April 1986, in final form 12 March 1987)

ABSTRACT

The release of freshwater from a midlatitude estuary to the continental shelf is modeled numerically as a Rossby adjustment problem using a primitive equation model. As the initial salinity front is relaxed, a first baroclinic-mode Kelvin wave propagates into the estuary, while along the continental shelf, the disturbance travels in the direction of coastally trapped waves but with a relatively slow propagation speed.

When a submarine canyon extends offshore from the estuary, the joint effect of baroclinicity and bottom relief provides forcing for barotropic flow. The disturbance now propagates along the shelf at the first coastally trapped wave-mode phase speed, and the shelf circulation is significantly more energetic and barotropic than in the case without the canyon.

For both the experiments with and without a canyon an anticyclonic circulation, generated by the surface outflow and deeper inflow over changing bottom topography, is formed off the mouth of the estuary. As the deeper inflow encounters shallower depth, the column of fluid is vertically compressed, thereby spinning up anticyclonically due to the conservation of potential vorticity. This feature is in qualitative agreement with the Tully eddy observed off Juan de Fuca Strait.

A study of the *reverse estuary* (where the estuarine water is denser than the oceanic water) shows that this configuration has more potential energy available for conversion to kinetic energy than the normal estuary. Bass Strait may be considered as a possible *reverse estuary* for generating coastally trapped waves.

The effects of a wider shelf and a wider estuary are examined by two more experiments. For the wider shelf, the resulting baroclinic flow is similar to that of the other runs, although the barotropic flow is weaker. The wide estuary model proves to be the most dynamic of all, with the intensified anticyclonic circulation now extending well into the estuary.

1. Introduction

The mainline of theoretical continental shelf circulation research has been along wind-forced coastally trapped wave models (e.g., see the reviews of Mysak, 1980; Allen, 1980). In these studies, the continental shelf is usually assumed uniform in the alongshore direction. In reality, the coastline is often interrupted by estuaries. The influence of buoyancy flux from the estuarine outflow on the continental shelf circulation is not well understood.

Two approaches have been used in the modeling of estuarine outflow onto the continental shelf. Csanady (1978), Beardsley and Hart (1978) and Beardsley and Winant (1979) have modeled the estuarine influence on the shelf circulation by sources or sinks of volume or vorticity along the coastline. Using barotropic or two-layer models, these studies of limited vertical structure concentrated on the steady-state horizontal shelf circulation induced by the sources/sinks on the coastal boundary, with the motion inside the estuary ignored. In contrast, Ou (1984), Wang (1984) and Van Heijst (1985) studied steady shelf-slope fronts with two-dimensional models in the xz-plane, where x and z are the offshore and vertical coordinates. By using a three-dimensional numerical model in this paper, we not only combine the two aforementioned types of models, but also enable the study of transient motions.

Fresh water runoff often increases suddenly over a week or less (e.g., in association with ice melting). This situation is modeled here by the Rossby adjustment problem in the absence of external forcing (Gill, 1976, 1982; Hsieh and Gill, 1984), where at time $t = 0$, the vertical dam at the mouth of the estuary is rapidly removed, and the fresh estuarine water is allowed to interact with the denser oceanic water. This "dam break" technique therefore gives a good sense of the time development of the response from an initial rest state.

Many estuaries, e.g., Juan de Fuca Strait off the coast of British Columbia, have submarine canyons extending offshore from the mouth of the estuary. We examine the effects of this canyon topography on the adjustment process.

In some areas, strong evaporation causes the estuarine water to be more saline than the oceanic water. The adjustment process for this *reverse estuary* (or *inverse estuary*) is compared with the normal estuary.

The outline of this paper is as follows: Section 2

* Also affiliated with: Institute of Applied Mathematics, University of British Columbia.

describes the numerical model used. The adjustment of fresh estuarine outflow (in the absence of a canyon) is studied in section 3, and in the presence of a canyon in section 4. The *reverse estuary* is examined in section 5. Two sensitivity studies are made in section 6, with a wider estuary and a wider shelf. Section 7 discusses some of the basic dynamics and energetics of the adjustment process, as well as some applications to the Tully eddy off Juan de Fuca Strait (Tully, 1942; Freeland and Denman, 1982), and the Australian Coastal Experiment (Freeland et al., 1986), where the Bass Strait is considered as a possible *reverse estuary* generating coastally trapped waves. A summary is presented in section 8.

2. Configurations used in the numerical model

The geometry of the estuary and shelf used in the first and third experiments is depicted in Fig. 1, with the initial salinity front indicated. Figure 2 illustrates the geometry used in the second and fourth experiments, where a submarine canyon extends offshore from the mouth of the estuary. The steep-sloping continental shelf used in all four of these runs is typical of the west coast of the North American continent. In Fig. 3, the cross-shelf topography and the initial vertical distributions of temperature and salinity, typical of Northeast Pacific summertime conditions, are shown (Halpern and Holbrook, 1972, p. 330; Holbrook and Halpern, 1974, p. 286; Emery and Dewar, 1982, p. 273 and p. 276).

In the fifth experiment we examined the effects of a wider shelf. The topography profile used is similar to that of Figs. 1 and 3, with the offshore width of each level approximately doubled. The influence of the estuary width on the continental shelf circulation was examined by means of a sixth experiment, with a 130-km wide estuary. The shelf topography used was identical to that of the first experiment (Figs. 1, 3).

The geostrophic adjustment process was investigated using the Cox (1984) version of the GFDL Bryan-Cox primitive equation model, with five vertical levels. Variable grid spacing was used to focus on the region near the mouth of the inlet where a 10 km by 10 km grid was incorporated. The grid spacing in the north-

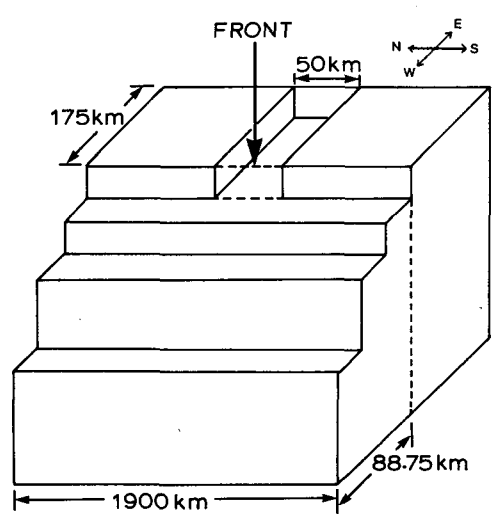

FIG. 1. Schematic diagram of the topography used in models without a canyon. The solid boundaries, 950 km north and south of the center of the estuary and 300 km offshore, are not shown.

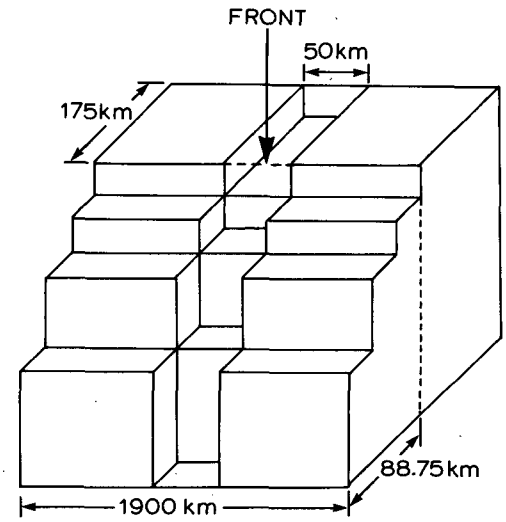

FIG. 2. As in Fig. 1, but used in models with a submarine canyon.

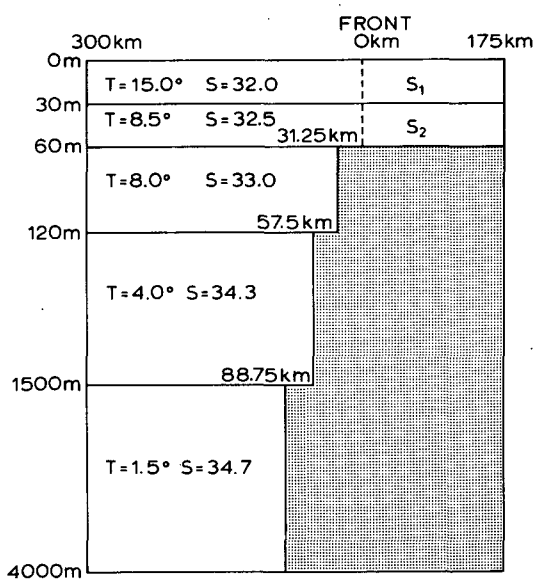

FIG. 3. East–west section of the model taken at the center of the estuary. The initial temperature and salinity data used and the shelf topography are indicated. The initial temperature distribution was horizontally uniform, but there was a discontinuity of the salinity across the front. For the fresh estuary model $S_1 = 30.0$, $S_2 = 30.5$. For the *reverse estuary* model $S_1 = 34.0$, $S_2 = 34.5$.

south direction was increased monotonically to a maximum of 100 km at the northern and southern solid boundaries, 950 km from the center of the inlet at 45°N. In the east–west direction the grid size was increased to a maximum of 30 km at the western solid boundary, 300 km offshore, and to 20 km at the eastern inlet boundary. All six experiments were relaxed without external forcing for ten days with a time step of 15 min. The lateral eddy viscosity and diffusivity were set at 1.0×10^7 and 4.0×10^6 cm^2 s^{-1}, respectively, while the vertical viscosity and diffusivity were both set at 1.0 cm^2 s^{-1}. Sensitivity tests were done with viscosities and diffusivities an order of magnitude greater and less than the aforementioned. The results presented in this paper proved to be relatively insensitive to the viscosities and diffusivities. Unrealistically large viscosities, however, caused damping of the results as expected.

In the following analysis the first experiment is used as a control for comparison with the other five experiments.

3. Relaxation in the absence of a canyon

The first experiment (with no canyon) was the relaxation of the initial density front at the mouth of a fresh estuary in the absence of external forcing. The vertical velocity field at 30 m depth at days 1 and 10 is plotted in Fig. 4. The initial adjustment process generated a first-mode baroclinic Kelvin wave front, with baroclinic Rossby radius $R \sim 30$ km, which propagated eastward along the southern wall of the estuary at a phase speed $c \sim 12$ km day^{-1}. The offshore grid spacing of 10 km used in the model is about twice the theoretical two-layer model Rossby radius ($\sim$5 km). This, combined with lateral viscosity used in the numerical model, produces a baroclinic Kelvin wave with much larger Rossby radius ($R \sim 30$ km) and slower phase speed than the theoretical results ($R \sim 5$ km and $c \sim 43$ km day^{-1}). This numerical effect has been examined in Hsieh et al. (1983). Along the continental shelf, coastally trapped waves are seen propagating northward in Fig. 4.

The transport streamfunction ψ is defined by

$$\psi_y = -\int_{-h}^{0} u\,dz, \quad \psi_x = \int_{-h}^{0} v\,dz, \tag{1}$$

where h is the depth and u and v, the eastward and northward velocity components respectively. Figure 5 shows the ψ field at days 1 and 10, while Fig. 6, a space–time contour plot, reveals the temporal variations of ψ along a north–south section located 65 km offshore. Soon after the start of the relaxation, near-inertial oscillations of period 17 h are seen propagating northward at around 450 km day^{-1} (Fig. 6), as an alternating series of cyclonic and anticyclonic cells (Fig. 5a). Overall, the

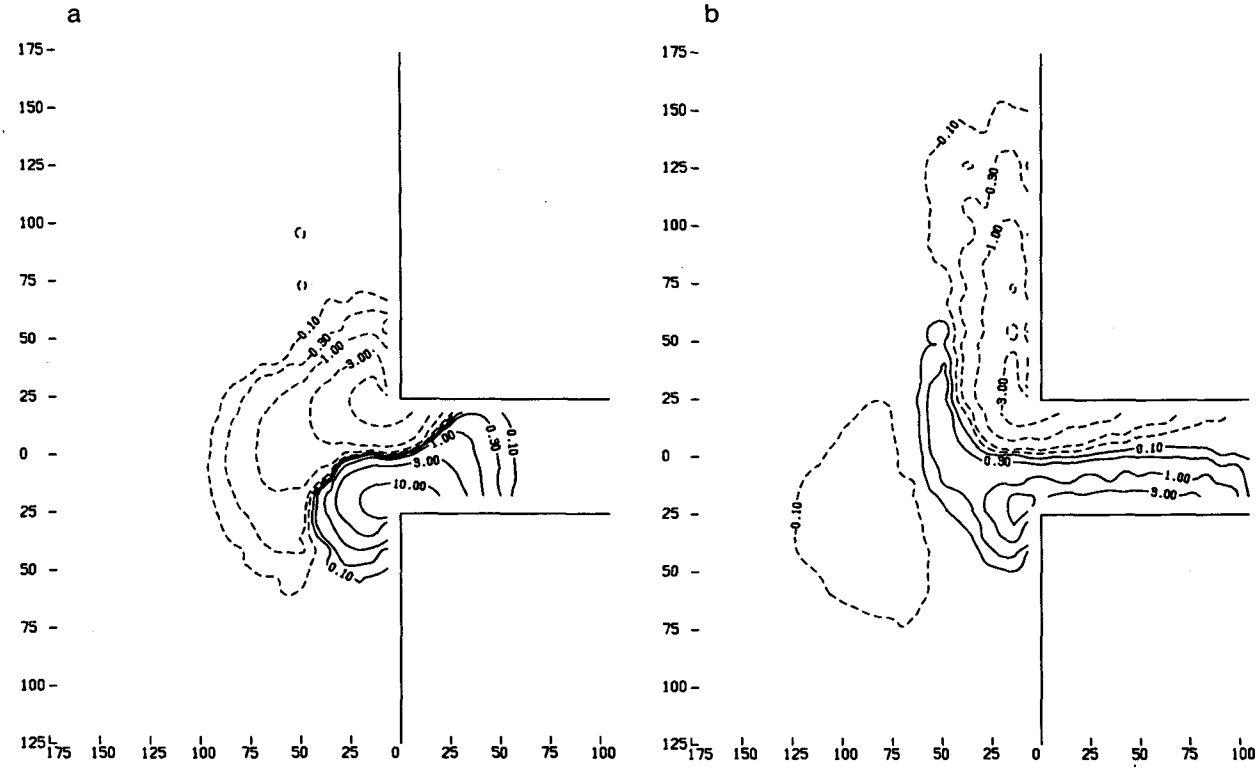

FIG. 4. Vertical velocity w (10^{-3} cm s^{-1}), at the interface between the first two levels (z = 30 m), for experiment 1 (the fresh estuary without a canyon), (a) t = 1 day, (b) t = 10 days. The vertical and horizontal axes are in km. The baroclinic flow field manifested in these plots indicates the propagation of a first-mode baroclinic Kelvin wave into the estuary.

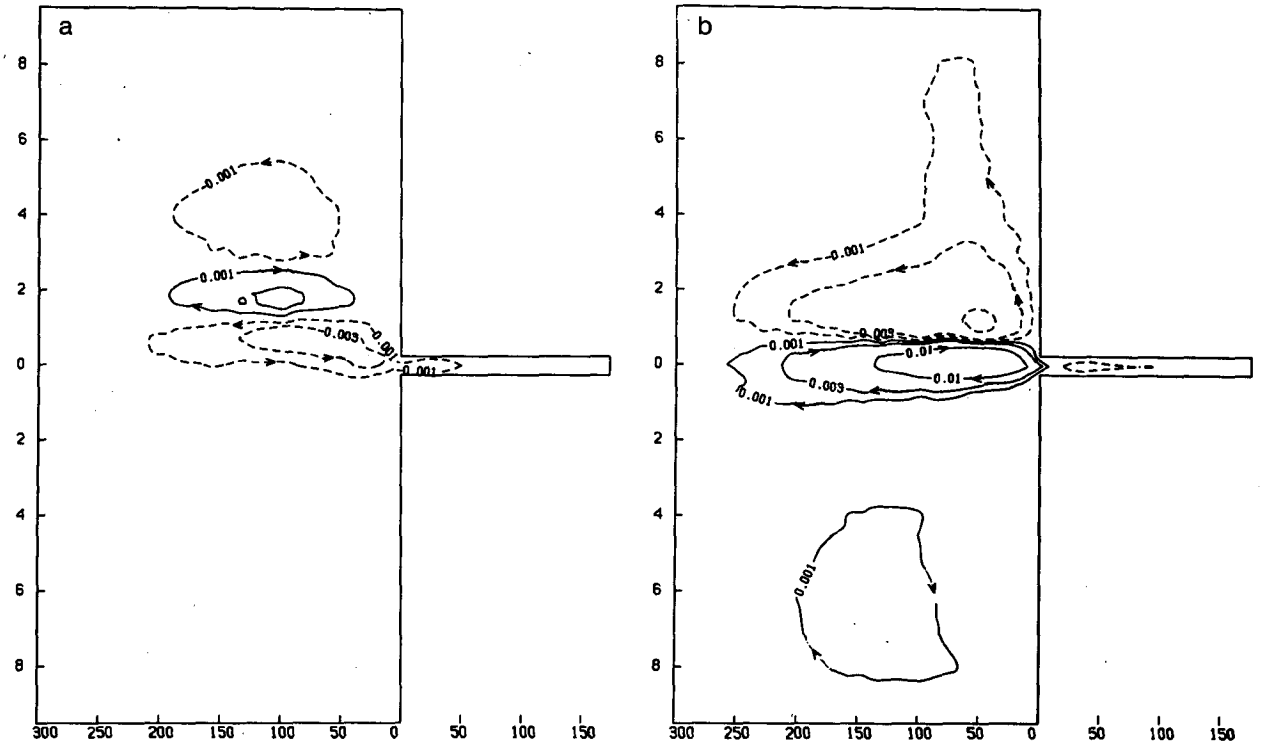

FIG. 5. Transport streamfunction ψ (Sv) at, (a) t = 1 day, (b) t = 10 days, for experiment 1. The vertical axis is in 10^2 km and the horizontal axis is in km. Coastally trapped waves propagate northward and a strong anticyclonic circulation, with large offshore extent, develops at the mouth of the inlet in (b).

northward propagation of the disturbances is rather slow and weak. After day 2, an anticyclonic circulation develops near the mouth of the estuary (Fig. 6), intensifying and extending offshore with time (Fig. 5b).

Figure 7 focuses on the horizontal velocity field in the vicinity of the salinity front. In the upper layer (Fig. 7a) the less-saline estuarine water flowed out of the inlet and progressed northward along the coast, whereas

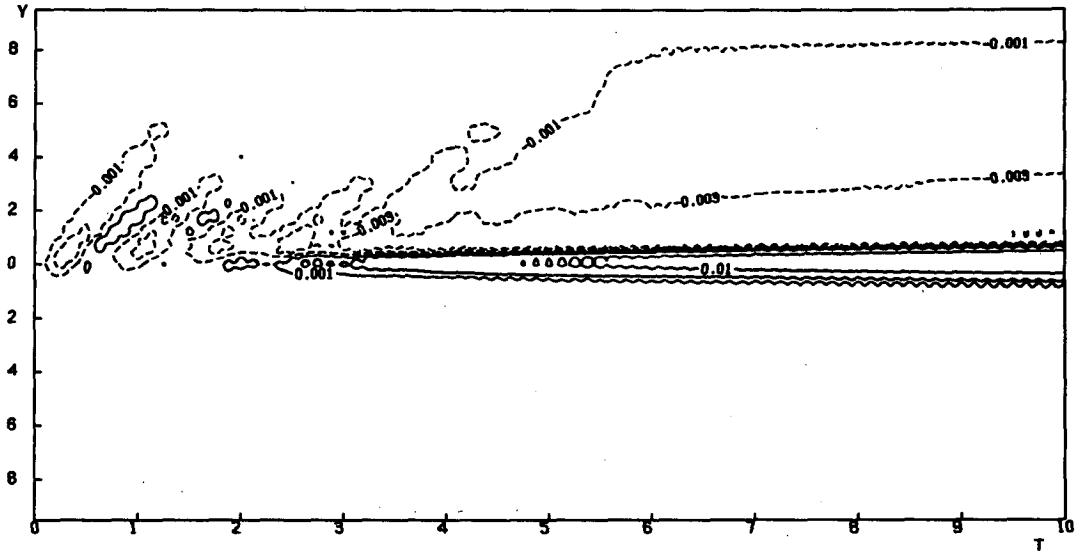

FIG. 6. Space–time plot of transport streamfunction ψ (Sv), along a north–south section 65 km offshore, for experiment 1. The top of the graph is the northern boundary. The vertical axis is in 10^2 km and the horizontal axis is in days. Northward phase propagation of the coastally trapped waves can clearly be seen.

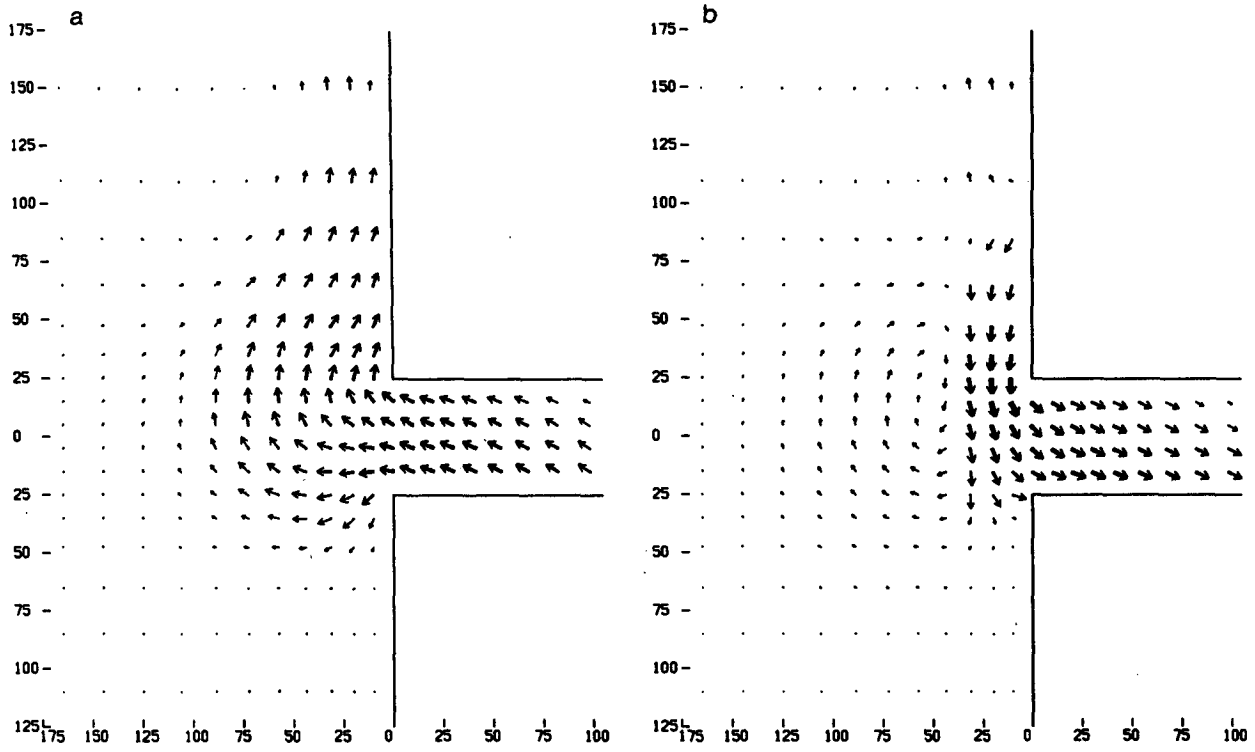

FIG. 7. Horizontal velocity field at ten days for experiment 1, (a) upper level (z = 15 m), (b) second level (z = 45 m). The magnitude of the velocity is proportional to the thickness and length of the vector. Both the vertical and horizontal axes are in km. A shelf-trapped eddy is observed in (b), just outside the estuary.

in the lower layer, the denser ocean water flowed in (Fig. 7b). Comparing the velocity fields in Figs. 7a and 7b, we find that in the northern shelf region, the flow established after the passage of the coastally trapped waves is quasi-barotropic, while the Kelvin wave inside the inlet produces a baroclinic flow. The anticyclonic circulation, mentioned above, appears in Fig. 7b trapped against the shelf break 55 km offshore. This is consistent with the conservation of potential vorticity, where a column of water in the lower layer, flowing eastward into the inlet, vertically contracts over the shallowing topography, and spins up in an anticyclonic sense.

4. Relaxation in the presence of a canyon

To examine the effects of topography on the relaxation process more closely, a canyon was introduced into the model. The resulting baroclinic flow field in the estuary was similar to that of section 3 in that a baroclinic Kelvin wave was generated, propagating eastward with a phase speed $c \sim 12$ km day^{-1}. North of the estuary the presence of the coastally trapped waves was also evident.

Comparing Figs. 8a, b with Figs. 5a, b, we find that in the presence of the canyon a much stronger barotropic circulation has developed within one day (Fig. 8a). A cyclonic flow was generated throughout the whole northern region of the model and an intense anticyclonic circulation was trapped in the mouth of the estuary. Contrary to section 3, the inlet-trapped anticyclonic circulation did not spread extensively offshore (Fig. 8b).

In Fig. 9, a streamfunction space–time plot across the same north–south section as in Fig. 6, the first coastally trapped wave mode is manifested in the 0.001 and 0.003 Sv contours (Sv $\equiv 10^6$ m^3 s^{-1}), which show northward propagation with $c \sim 600$ km day^{-1}. Figure 9 suggests the dominance of the first mode in the presence of the canyon, a situation not found in the absence of a canyon (Fig. 6).

Several differences between the net velocity field considered in section 3 and the present case are illustrated in Figs. 10a, b (cf. Figs. 7a, b). Due to dominance of the first mode, the magnitude of the barotropic flow was much greater when the canyon was present. This can be seen in the two second-level plots, where the coastal baroclinic flow (manifested by a reversal from the upper level currents) is dominant up to about 110 km north, with no canyon, but only to 85 km north of the estuary with a canyon.

Comparing Fig. 10b with Fig. 7b, we note that the canyon caused the anticyclonic circulation to be trapped much closer to the mouth of the inlet. Once

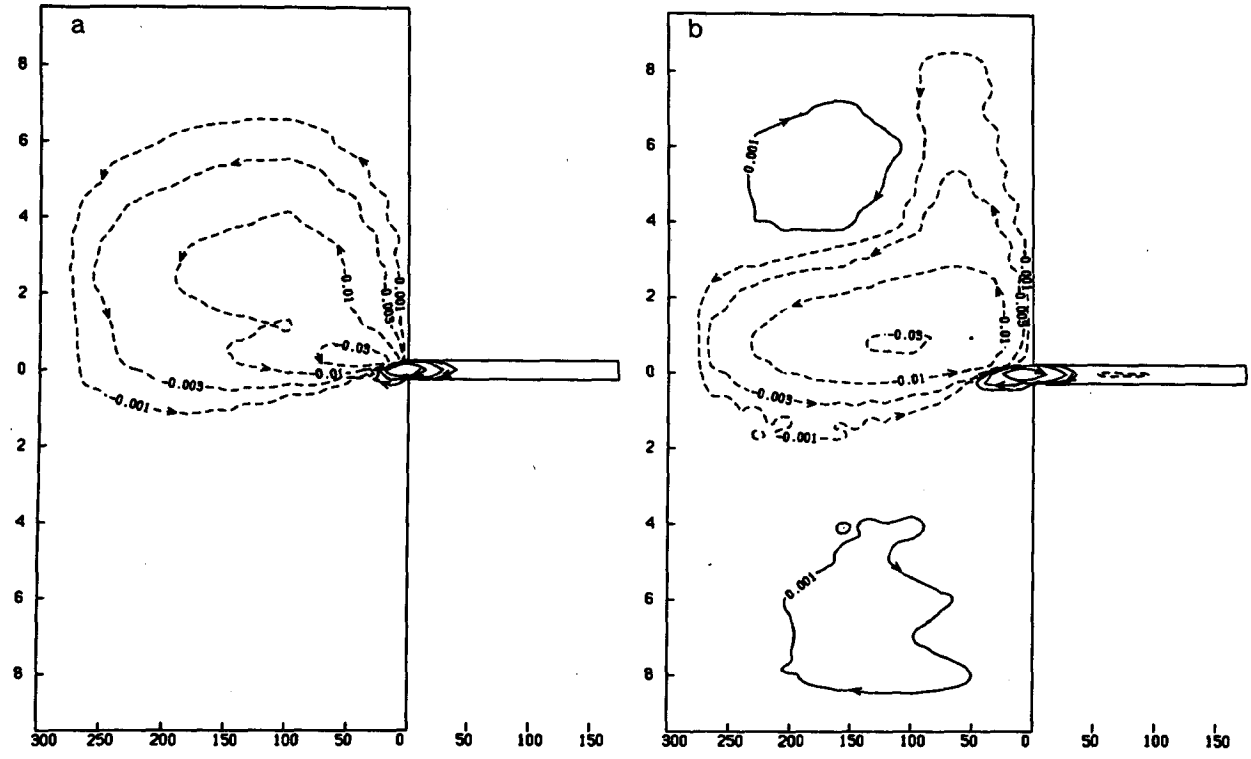

FIG. 8. Transport streamfunction ψ (Sv) at, (a) t = 1 day, (b) t = 10 days, for experiment 2 (the fresh estuary with a canyon). The vertical axis is in 10^2 km and the horizontal axis is in km. A coastally trapped wave front propagates northward and a strong anticyclonic circulation is trapped at the mouth of the estuary.

more, conservation of potential vorticity provides a mechanism for the circulation's existence and location—with the canyon, the most rapid compression of the inflowing lower column of water occurs much closer to the mouth of the inlet, hence the new location of the anticyclonic circulation. Figures 10a, b also show

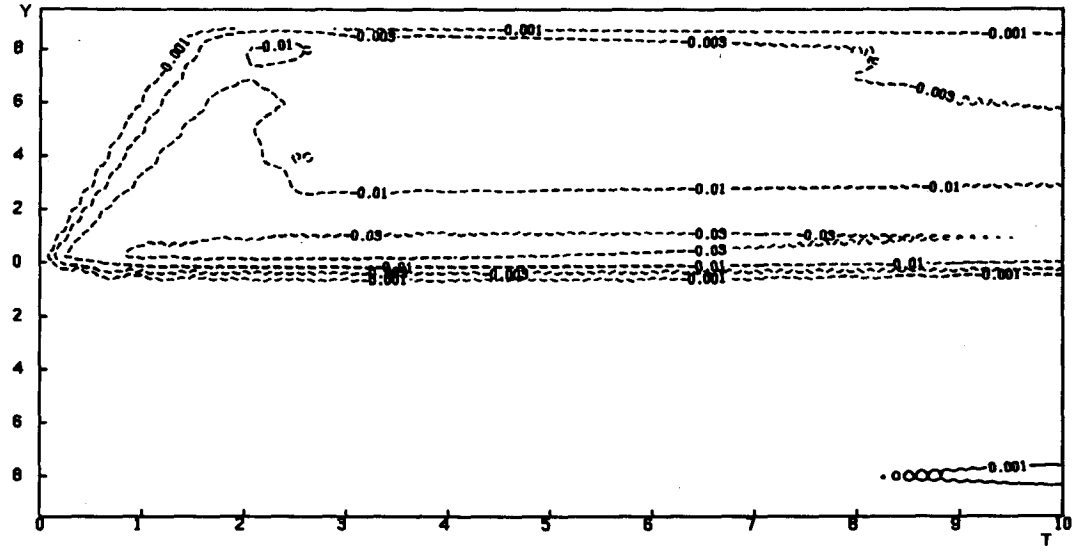

FIG. 9. Space–time plot of transport streamfunction ψ (Sv), along a north–south section 65 km offshore, for experiment 2. The top of the graph is the northern boundary. The vertical axis is in 10^2 km and the horizontal axis is in days. A first-mode coastally trapped wave front is now clearly observed (cf. Fig. 6).

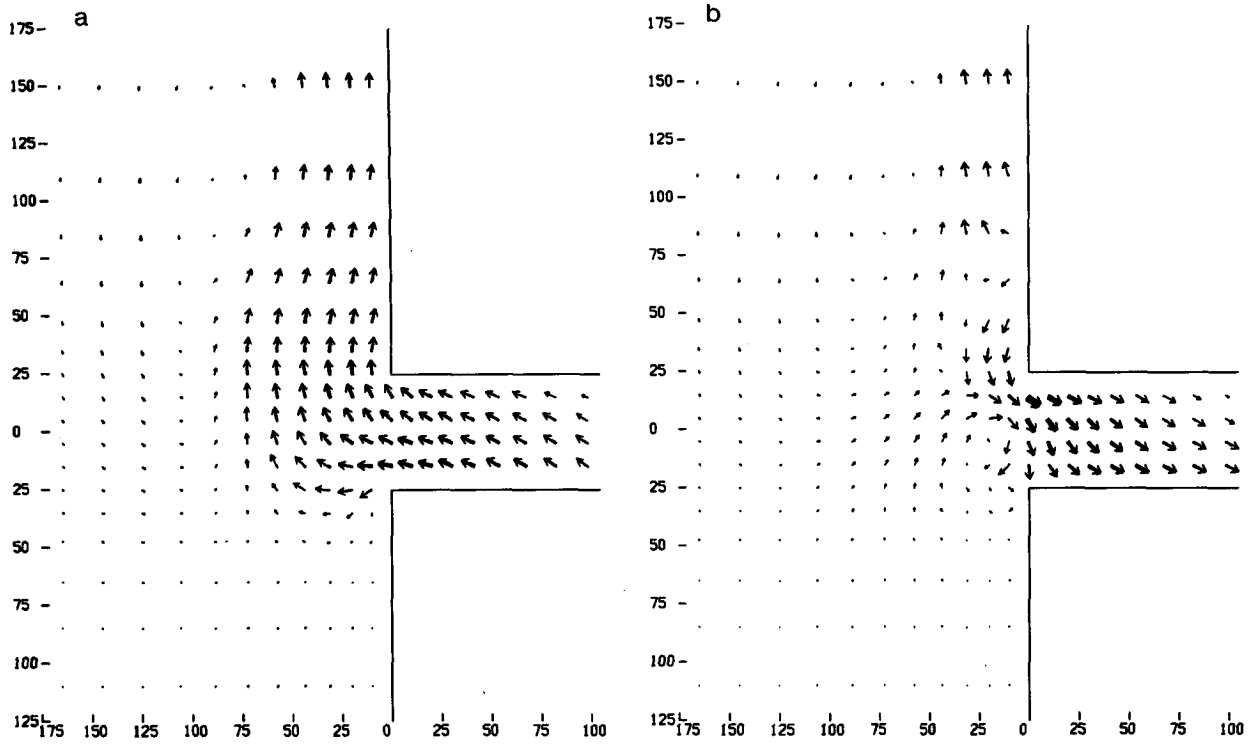

FIG. 10. Horizontal velocity field at ten days for experiment 2, (a) upper level, (b) second level. Both the vertical and horizontal axes are in km. The anticyclonic eddy is now trapped at the mouth of the inlet.

that the canyon had little effect on the generation and propagation of the first-mode baroclinic Kelvin wave into the estuary (cf. Figs. 7a, b).

5. Reverse estuaries

For the *reverse estuary,* the first and second experiments were repeated with the estuarine water more saline than the oceanic water at corresponding depth (Fig. 3). The general circulation was similar to that depicted in Figs. 4–10, although more available potential energy was converted into kinetic energy (section 6) and the direction of the flow was basically reversed.

In both experiments a first-mode baroclinic Kelvin wave was generated at the mouth of the inlet and was observed to propagate into the estuary with $c \sim 12$ km day^{-1}. In the presence of a canyon the first coastally trapped mode appeared dominant in the northern velocity field, whereas with no canyon present the first mode was not dominant.

The eddy trapped at the shelf break (Fig. 7b) was also present in the *reverse estuary* experiments except its direction was reversed. Similarly, when a canyon was added, the cyclonic eddy was trapped near the mouth of the inlet as in Fig. 10b, but with the direction reversed. Both the above observations are once more consistent with the conservation of potential vorticity—in the *reverse estuary,* a column of deeper water flows out of the inlet, and vertically stretches over the deepening topography, with a corresponding cyclonic spinup.

6. Experiments with a wider shelf and a wider estuary

In the fifth experiment we examined the effects of a wider shelf. The baroclinic flow field remained largely unchanged, although it extended further offshore in the current field. There was less energy transferred into barotropic motion as is evident in Figs. 11a, b (cf. Figs. 5b, 6). Near-inertial oscillations of period 17 h propagated northward soon after the start of the relaxation process (Fig. 11b) as in Fig. 6, but now with a faster phase speed and greater offshore extent, as expected for coastally trapped waves on a wider shelf. A large anticyclonic circulation was once more trapped at the shelf break 88.75 km offshore (as opposed to 57.5 km).

The model response is much more sensitive to a change in the width of the estuary. Experiment 6 was run with an estuary 130 km wide (as opposed to 50 km). The resulting motion was more energetic than the narrow estuary case, since the wider estuary had a larger initial reservoir of fresh water and hence more available potential energy.

In the case with the narrow estuary, the Kelvin wave completely dominated the baroclinic motion inside the estuary (Fig. 4b). In the wide estuary, there are alter-

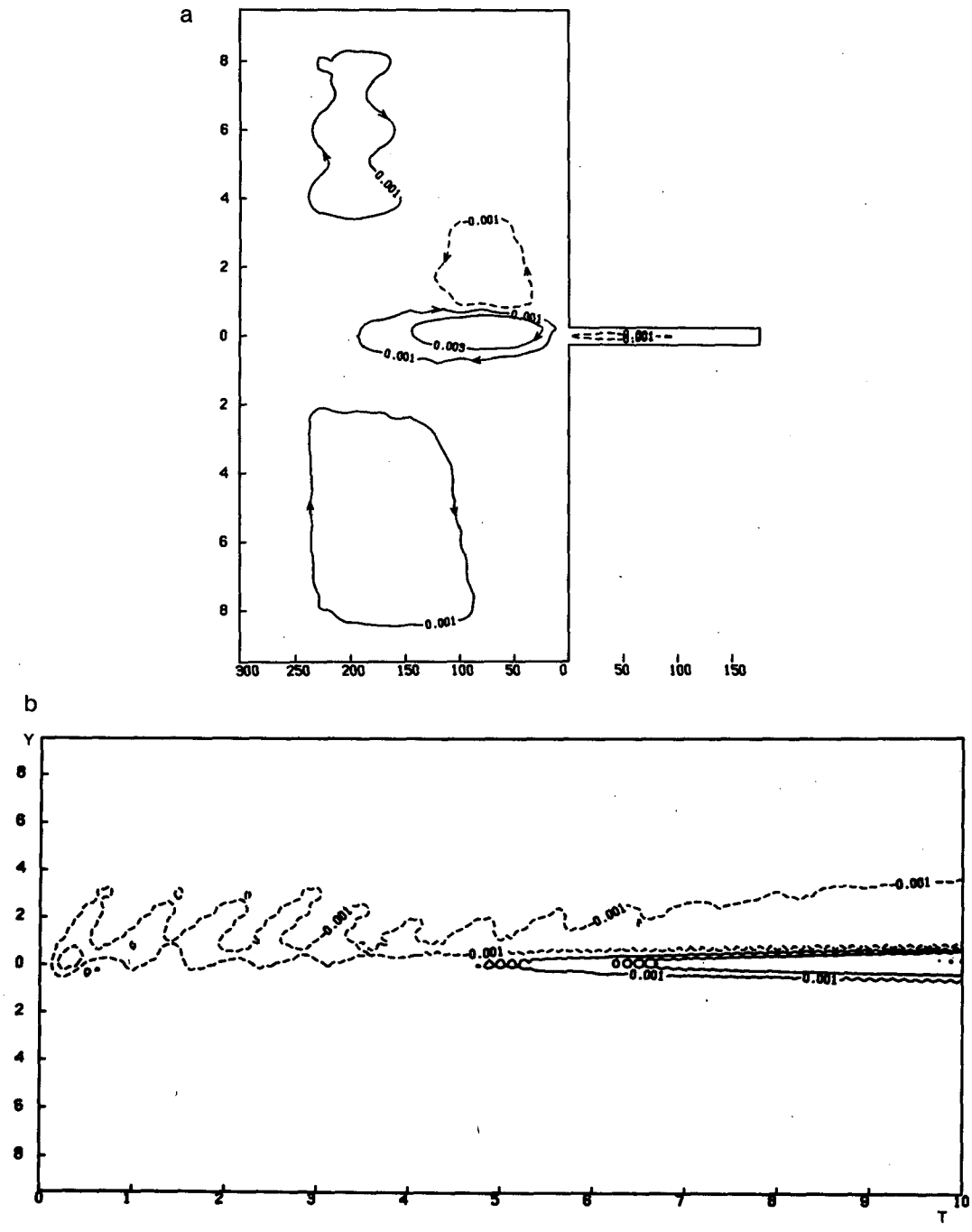

FIG. 11. Transport streamfunction ψ (Sv) for experiment 5 (the wider shelf). (a) t = 10 days. The vertical axis is in 10^2 km and the horizontal axis is in km. (b) Space–time plot along a north–south section 65 km offshore. The top of the graph is the northern boundary. The vertical axis is in 10^2 km and the horizontal axis is in days.

nating patches of upwelling and downwelling across the channel (Fig. 12), suggesting the excitation of Poincaré modes in addition to the Kelvin mode. From the dispersion relation of Poincaré waves (LeBlond and Mysak, 1978, p. 271), we know that for narrow channels, Poincaré modes are spatially evanescent. Even for a wide channel, the Poincaré modes form part of the transient response, since at low-enough frequency, the Poincaré waves are temporally decaying. The baroclinic field associated with the coastally trapped waves appears little affected by the change in the width of the estuary (Fig. 12, cf. Fig. 4b).

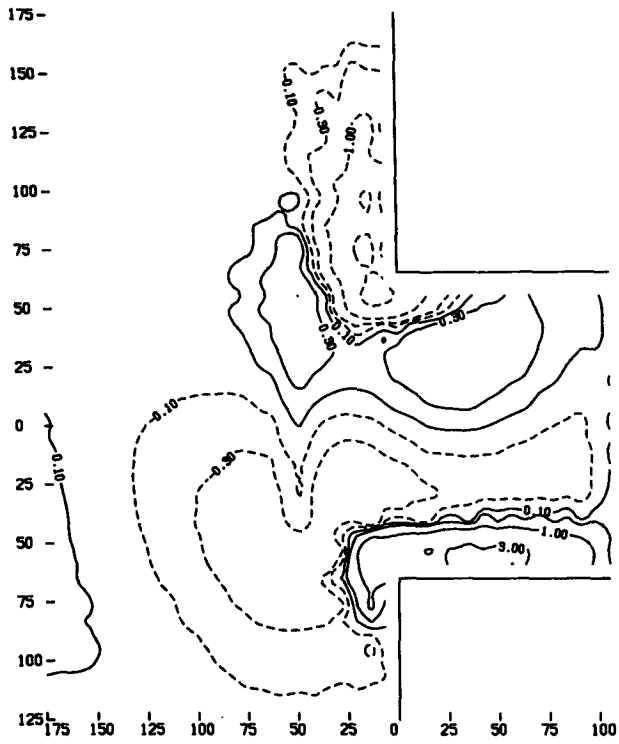

FIG. 12. Vertical velocity w (10^{-3} cm s^{-1}), at the interface between the first two levels (z = 30 m), for experiment 6 (the wide estuary) at t = 10 days. The vertical and horizontal axes are in km.

The barotropic motion was much more energetic for the wide estuary model than for the narrow estuary model. Figure 13a illustrates the streamfunction ψ at 10 days. The large anticyclonic circulation which now extends well into the estuary itself is much stronger than that in Fig. 5b. The alternating cyclonic–anticyclonic cell pattern observed in Fig. 5a was also present in the wide estuary case, although the circulation was stronger and had greater northward extent, as seen in Fig. 13b, a space–time plot across the same section as Fig. 6.

The velocity field at 10 days is depicted in Figs. 14a, b for the wide estuary case. The large anticyclonic circulation in the lower layer (Fig. 14b) is once more evident at the shelf break (cf., Fig. 7b). Inside the estuary there exists an anticyclonic eddy in the upper layer (Fig. 14a) which was not apparent in the narrow estuary case (Fig. 7a), where the Kelvin wave dominated the estuarine circulation.

7. Discussion

We now consider how barotropic circulation is generated from the initial density front. Here for simplicity we use the governing momentum equations in Cartesian form.

$$\frac{Du}{Dt} - fv = -\frac{1}{\rho_0} p_x + \nu(u_{xx} + u_{yy}) + \kappa u_{zz}, \tag{2}$$

$$\frac{Dv}{Dt} + fu = -\frac{1}{\rho_0} p_y + \nu(v_{xx} + v_{yy}) + \kappa v_{zz}, \tag{3}$$

$$p_z = -\rho g, \tag{4}$$

where x is oriented eastward and y northward. The constants ν and κ are the lateral and vertical viscosities, respectively. Depth averaging the linearized, inviscid versions of (2) and (3), substituting in (1) and taking the curl, we obtain

$$\left(\frac{1}{h}\psi_{yt}\right)_y + \left(\frac{1}{h}\psi_{xt}\right)_x + \left(\frac{f}{h}\psi_x\right)_y - \left(\frac{f}{h}\psi_y\right)_x = \left[\frac{g}{\rho_0 h}\int_{-h}^{0}\int_{z}^{0} \rho_x dz'dz\right]_y - \left[\frac{g}{\rho_0 h}\int_{-h}^{0}\int_{z}^{0} \rho_y dz'dz\right]_x, \tag{5}$$

where (4) has been written as,

$$p(z) = p_s + \int_z^0 g\rho dz', \tag{6}$$

with p_s the rigid-lid surface pressure. Equation (5) is a wave equation for barotropic motion, with the forcing term on the right-hand side arising from the joint effect of baroclinicity and relief (JEBAR). For the application herein f is constant and *initially* $\rho = \rho(x, z)$, so that at the initial moment (5) reduces to,

$$\{\psi_{yyt} + \psi_{xxt}\} - \frac{1}{h}\{h_y\psi_y + h_x\psi_x\}_t - \frac{f}{h}\{h_y\psi_x - h_x\psi_y\} = \frac{gh_y}{\rho_0}\left\{\frac{-1}{h}\int_{-h}^{0}\int_{z}^{0} \rho_x dz'dz + \int_{-h}^{0} \rho_x dz\right\}. \tag{7}$$

In the models without the canyon, $h = h(x)$, the forcing term vanishes from (7), hence only weak barotropic flow is observed. With the canyon, h_y is nonzero, and the JEBAR term produces a much stronger barotropic circulation, with the emission of coastally trapped wave fronts as in Hsieh and Gill (1984).

The *reverse estuary* experiments produced more energetic flows than the fresh estuary experiments, despite having initial salinity fronts of equal strength. This can be accounted for by the difference in the available potential energy in the two cases. In the *reverse estuary* models, dense water from the estuary flowed down the shelf to a considerable depth, whereas the rearrangement of water masses in the fresh estuary cases was restricted to the top two levels, hence a more limited conversion of potential to kinetic energy. The ratio between the steady state (assuming no viscosity) total kinetic energy of the reverse and fresh estuary models was estimated using

$$\mathrm{KE}_{ssr}/\mathrm{KE}_{ssf} = \mathrm{APE}_r/\mathrm{APE}_f, \tag{8}$$

where APE_r and APE_f are the available potential energies of the *reverse* and fresh estuary models, respectively. The available potential energies were calculated

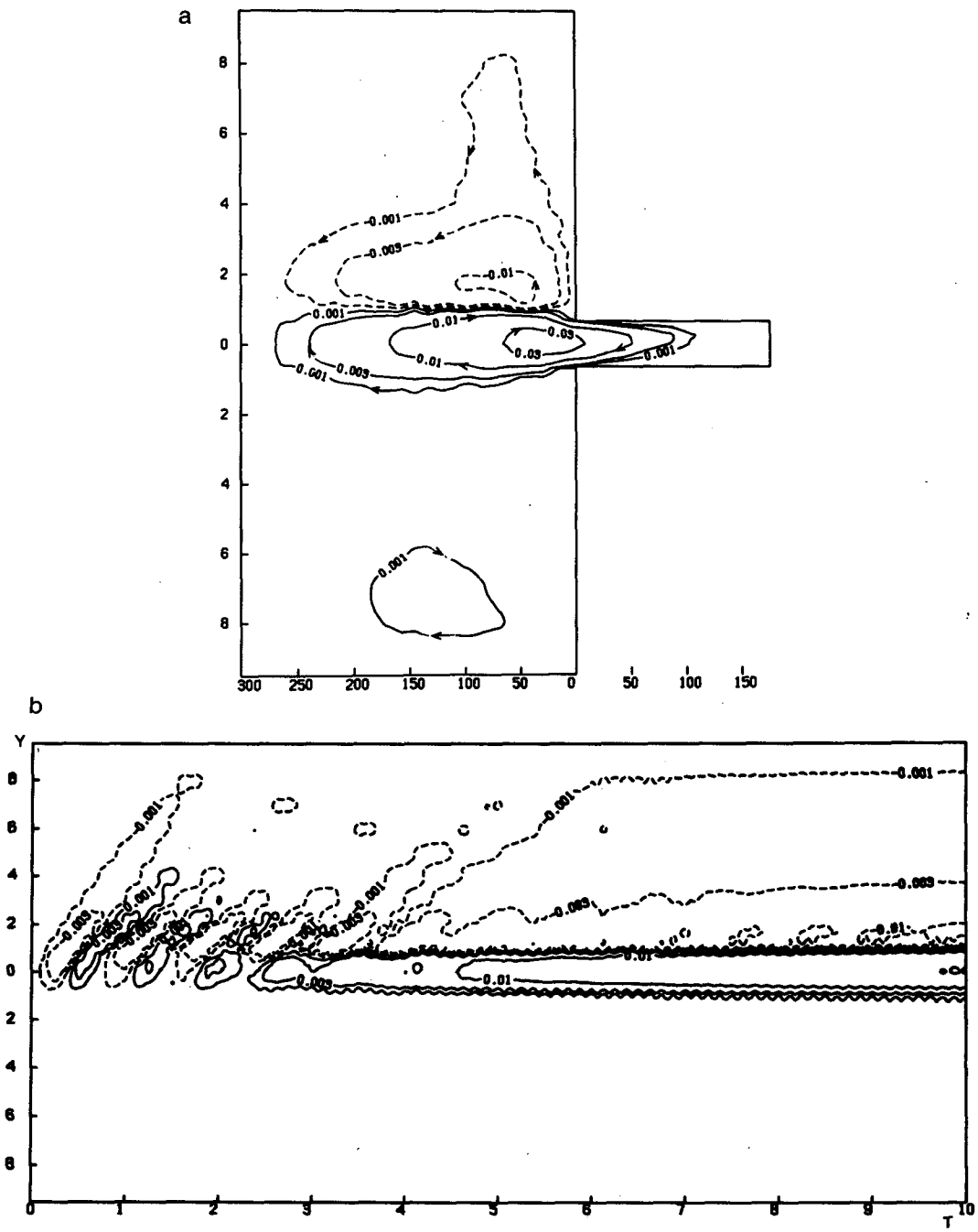

FIG. 13. Transport streamfunction ψ (Sv) for experiment 6. (a) t = 10 days. The vertical axis is in 10^2 km and the horizontal axis is in km. (b) Space–time plot along a north–south section 65 km offshore. The top of the graph is the northern boundary. The vertical axis is in 10^2 km and the horizontal axis is in days.

using a simple slab model. The water masses of fixed density were assumed to move without mixing from the initial configuration to the final state where the slabs of water masses laid on top of each other, with the denser ones below. We let

$$\mathrm{APE} = \int_V (\rho_i - \rho_f) g z dV, \tag{9}$$

where ρ_i and ρ_f are the initial and final densities. This somewhat simple calculation yielded,

$$\mathrm{APE}_r/\mathrm{APE}_f \sim 2, \tag{10}$$

i.e., the *reverse estuary* had nearly twice the available potential energy of the fresh estuary.

For idealized situations, the APE for fresh and re-

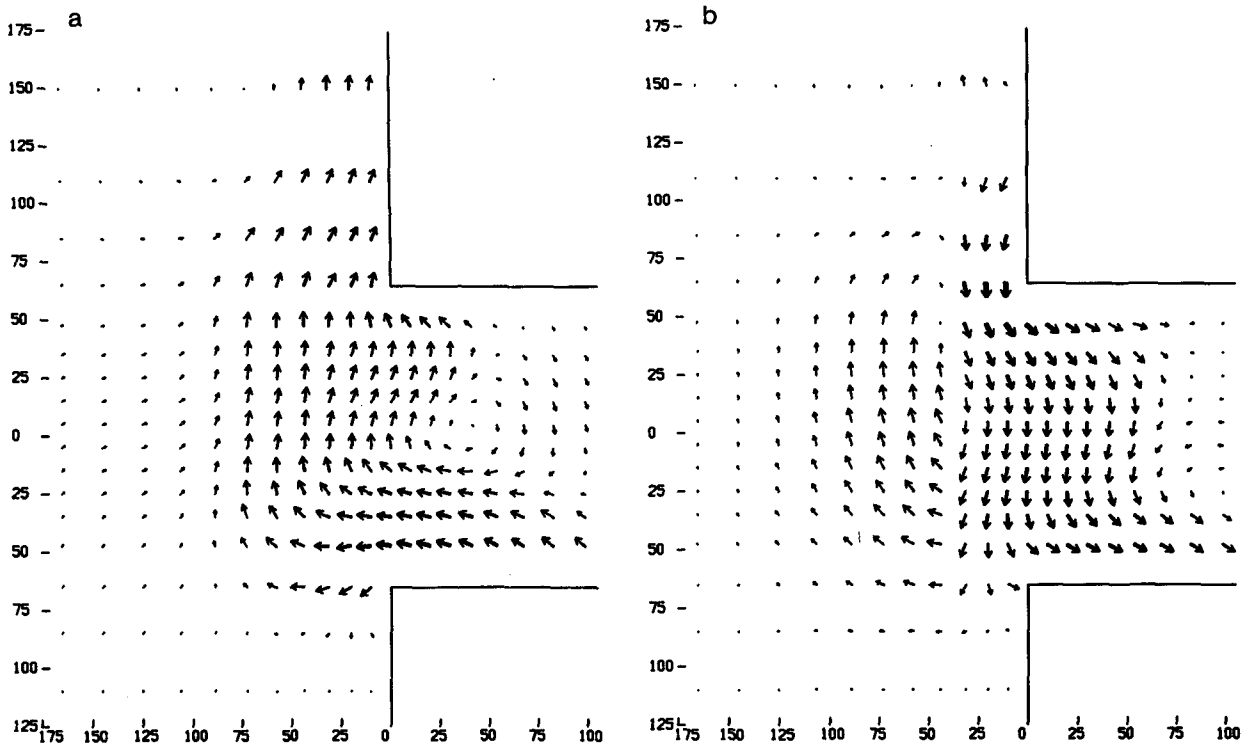

FIG. 14. Horizontal velocity field at ten days for experiment 6, (a) upper level (z = 15 m), (b) second level (z = 45 m). The magnitude of the velocity is proportional to the thickness and length of the vector.

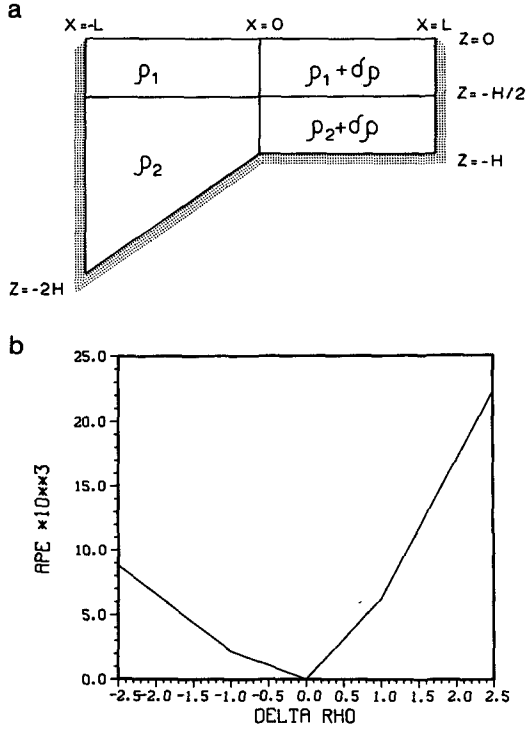

FIG. 15. (a) Simple linear slope model with ρ_1 = 1024.0, ρ_2 = 1025.0 kg m^{-3}, -2.5 kg m$^{-3} \leq \delta\rho \leq 2.5$ kg m^{-3} and H = 60 m. (b) Available potential energy per unit horizontal area in J m^{-2} as a function of $\delta\rho$ [see Eq. (11)].

verse estuaries can be calculated analytically. Consider the initial configuration of Fig. 15a, where the available potential energy per unit horizontal area, for given $\delta\rho$, was calculated using Eq. (9). Once more, water masses of fixed density were assumed to move without mixing from the initial state (Fig. 15a) to the final state. This calculation gave

$$\mathrm{APE} = \frac{gH^2}{16}\begin{cases} (\rho_1-\rho_2)-2\delta\rho, \\ \quad \text{if } \rho_1+\delta\rho \leq \rho_1,\ \rho_2+\delta\rho \leq \rho_1 \\ -\delta\rho, \quad \text{if } \rho_1+\delta\rho \leq \rho_1 \leq \rho_2+\delta\rho \leq \rho_2 \\ {}^{17}/_{6}\delta\rho, \quad \text{if } \rho_1 \leq \rho_1+\delta\rho \leq \rho_2 \leq \rho_2+\delta\rho \\ 2(\rho_1-\rho_2)-{}^{29}/_{6}\delta\rho, \\ \quad \text{if } \rho_1+\delta\rho \geq \rho_2,\ \rho_2+\delta\rho \geq \rho_2. \end{cases} \tag{11}$$

The available potential energy per unit area (11), plotted as a function of $\delta\rho$ in Fig. 15b, shows that the reverse estuary ($\delta\rho > 0$) has much greater available potential energy than the corresponding fresh estuary ($\delta\rho < 0$) of equivalent density difference ($|\delta\rho|$). Hence, the reverse estuary cases were more energetic than the fresh estuary cases.

Figure 16 illustrates the time progression of the total kinetic energy of the model ocean for all six experiments. The initially prevalent inertial oscillations

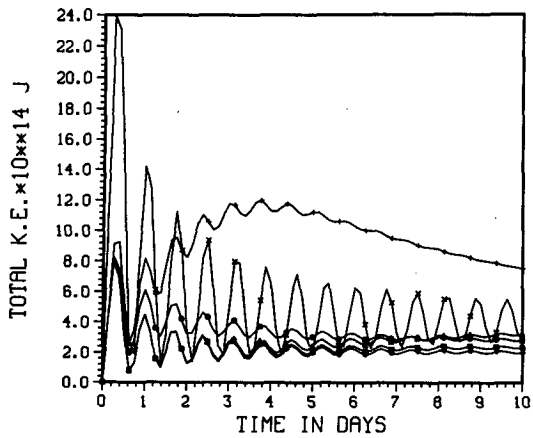

FIG. 16. Total kinetic energy (Joules) of the model ocean as a function of time: □—Fresh estuary with no canyon. ○—Fresh estuary with the canyon. △—*Reverse estuary* with no canyon. +—*Reverse estuary* with the canyon. ×—Wide fresh estuary with no canyon. ◇—Fresh estuary with no canyon and a wide shelf.

gradually diminish with time in all but the wide estuary experiment. Both experiments with the canyon have more kinetic energy than the corresponding experiments without the canyon. The *reverse estuary* with the canyon was by far the most energetic case. The dense fluid from the estuary, instead of flowing across the shelf, dropped directly into the canyon, thereby releasing much potential energy. The wide estuary run proved to be more energetic than the narrow estuary run due to the larger reservoir of fresh water and hence the more available potential energy. Even after ten days, inertial oscillations are prevalent in the wide estuary solution (Fig. 16).

Shelf-trapped eddies are commonly observed off the coast of British Columbia, the best documented of which is the Tully eddy (Tully, 1942; Freeland and Denman, 1982). This eddy is observed at the entrance to Juan de Fuca Strait during the summer months when runoff from the Fraser river is high, often doubling in magnitude over the period of a week in association with ice melting (Tully, 1942, Fig. 2). Figure 17 shows the approximate location of this eddy in relation to the mouth of Juan de Fuca Strait. The previous dynamic height observations found that the upper layer of the eddy moved cyclonically relative to the lower layer. Recent current meter observations during the summer of 1985 (P. C. McIntosh, personal communication, 1985) showed cyclonic circulation near the surface and a small anticyclonic circulation below. The observation that the deeper flow is anticyclonic relative to the surface flow is consistent with the mechanism proposed herein, namely the inflowing lower layer compresses vertically, with an anticyclonic spinup. The cyclonic circulation at the surface is not predicted by the model. Freeland and Denman (1982) postulated that this cyclonic circulation spins up during the "spring transition", a period when the shelf-edge currents reverse in direction. In winter the shelf-edge currents flow northwards and in summer they flow southwards.

The results from the Australian Coastal Experiment (ACE), conducted from September 1983 to March 1984, indicate the presence of coastally trapped waves (CTWs) along the eastern coast of New South Wales (Freeland et al., 1986). The work of Clarke and Thompson (1984) suggested that CTWs would be forced by the local wind stress. Freeland et al. (1986) therefore expected to see little or no signal at line 1 (Fig. 18) but at more northerly lines, the northward propagation of longshore currents at (350–450) km day^{-1} (the phase speed of a first-mode wave).

The experiment turned out to reject this hypothesis. A large CTW signal was observed at line 1 and Freeland et al. (1986) wrote, "The significant result from these calculations is the clear indication that the CTW signal appears to propagate from line 1 to 2 with little modification by the winds." There was, however, no CTW signal observed at Hobart (line 0), (Fig. 18). From a modal decomposition of the energy flux through a vertical section across line 1, Freeland et al. (1986) found the first three CTW modes contributed, 30.5%, 49% and 20.5%, respectively, to the total energy flux.

Bass Strait is about 250 km wide and has an average depth of 60 m. There are no large-scale topographic features (e.g., canyons) in its vicinity. Throughout the year, water in the Bass Strait is 1°–3°C colder than the surface waters of the Tasman Sea to the east, and in the Southern Hemisphere winter it is also 0.5–2.0 ppt more saline (Godfrey et al., 1980, Tomczak, 1985). It is well known that in winter the dense Bass Strait water flows down the continental shelf to as deep as 400 m below the surface (Boland, 1971; Tomczak, 1985).

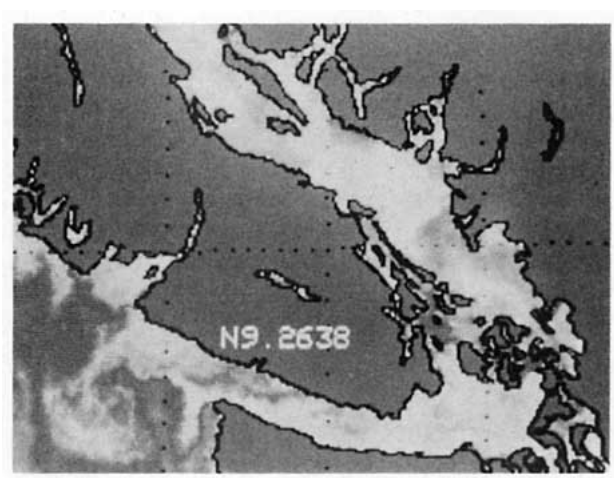

FIG. 17. Satellite image of Juan de Fuca Strait region off the west coast of British Columbia, taken at 0257 PST 17 June 1985. The Tully eddy is visible in the lower left corner of the diagram where the water is colder (whiter in the figure) than its surroundings.

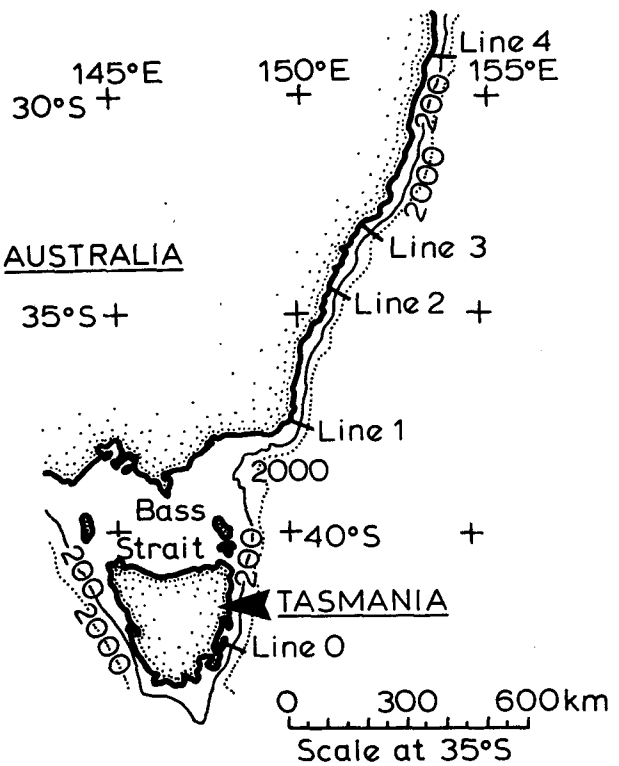

FIG. 18. Map of southeastern Australia indicating the five lines of current meter moorings in the Australian Coastal Experiment (redrawn from Freeland et al., 1985).

Godfrey et al. (1980) called this the Bass Strait winter cascade. This gives a possible mechanism for the generation of the CTWs which propagate along the coast of New South Wales. Using realistic topography, Weaver (1987) numerically simulated the flow of dense Bass Strait water onto the continental shelf. Though CTWs were generated, the magnitude of the alongshore velocities appeared to be somewhat lower than those observed in ACE.

8. Summary

We have modeled the sudden release of a large amount of fresh water from an estuary to the continental shelf as a Rossby adjustment problem. As the initial salinity front is relaxed, a first-mode baroclinic Kelvin wave front propagates into the estuary, while along the continental shelf, the disturbance propagates in the direction of coastally trapped waves. When the shelf is uniform in the alongshore direction, the propagation of the disturbance along the shelf is relatively slow and weak. In view of the nature of coastally trapped modes at midlatitudes where the first mode is often quasi-barotropic while the higher modes are more baroclinic (Brink, 1982), it seems probable that a baroclinic process like frontal relaxation does not feed much energy directly into the quasi-barotropic first mode.

When a submarine canyon is placed at the mouth of the estuary, the joint effect of baroclinicity and relief provides a strong forcing term for barotropic flow. The disturbance now propagates along the shelf at the first-mode phase speed, and the resulting circulation is significantly more energetic and barotropic than in the case without the canyon.

The surface outflow and the deeper inflow at the mouth of the estuary provide an interesting mechanism for eddy generation. As the deeper inflow encounters shallowing depth, the inflowing column of fluid is vertically compressed, thereby spinning up anticyclonically.

Comparing the *reverse estuary* with the normal estuary, we found that even when both estuaries had initial density fronts of equal magnitude, the *reverse estuary* managed to convert more of its potential energy into kinetic energy, thereby producing a stronger continental shelf circulation.

The introduction of a wider shelf had little effect on the resulting baroclinic circulation and as in the narrower shelf model, little energy was transferred into barotropic motion. The wide estuary experiment, on the other hand, proved to be far more energetic than the narrow estuary case due to the larger reservoir of fresh water available. The motion inside the wide estuary revealed the excitation of Poincaré modes in addition to the Kelvin mode. The coastally trapped waves appeared largely unaffected by changing the width of the estuary.

Acknowledgments. We are grateful to M. D. Cox for kindly providing us with the GFDL primitive equation model. We also thank R. K. Dewey and P. C. McIntosh for interesting discussions on recent field observations of the Tully eddy, and J. A. Church for suggesting the possible application of the model to Bass Strait. Finally, we thank A. C. Thomas for providing us with Fig. 17 and L. A. Mysak for his comments on the first draft. This research was supported by NSERC Strategic Grant G-1485, awarded to L. A. Mysak, K. Hamilton and C. Groot, for the study of the Meteorological and Oceanographic Influences on Sockeye Salmon Tracks (MOIST). An overview of this project can be found in Mysak et al. (1986).

REFERENCES

Allen, J. S., 1980: Models of wind-driven currents on the continental shelf. *Annual Reviews of Fluid Mechanics,* Vol. 12, Annual Reviews, 389–433.

Beardsley, R. C., and J. Hart, 1978: A simple theoretical model for the flow of an estuary onto a continental shelf. *J. Geophys. Res.,* **83,** 873–883.

——, and C. D. Winant, 1979: On the mean circulation in the Mid-Atlantic Bight. *J. Phys. Oceanogr.,* **9,** 612–619.

Boland, F. M., 1971: Temperature–salinity anomalies at depths between 200 and 800 m in the Tasman Sea. *Aust. J. Mar. Freshwater Res.,* **22,** 55–72.

Brink, K. H., 1982: A comparison of long coastal-trapped wave theory with observations off Peru. *J. Phys. Oceanogr.,* **12,** 897–913.

Clarke, A. J., and R. O. R. Y. Thompson, 1984: Large-scale wind-driven ocean response in the Australian Coastal Experiment region. *J. Phys. Oceanogr.*, **14,** 338–352.

Cox, M. D., 1984: A primitive equation, three-dimensional model of the ocean. GFDL Ocean Group Tech. Rep. No. 1.

Csanady, G. T., 1978: The arrested topographic wave. *J. Phys. Oceanogr.*, **8,** 47–62.

Emery, W. J., and J. S. Dewar, 1982: *Mean Temperature-Salinity, Salinity-Depth and Temperature-Depth Curves for the North Atlantic and the North Pacific.* Pergamon Press, 87 pp.

Freeland, H. J., and K. L. Denman, 1982: A topographically controlled upwelling center off southern Vancouver Island. *J. Mar. Res.*, **40,** 1069–1093.

——, F. M. Boland, J. A. Church, A. J. Clarke, A. M. G. Forbes, A. Huyer, R. L. Smith, R. O. R. Y. Thompson and N. J. White, 1986: The Australian coastal experiment: A search for coastal-trapped waves. *J. Phys. Oceanogr.*, **16,** 1230–1249.

Gill, A. E., 1976: Adjustment under gravity in a rotating channel. *J. Fluid. Mech.*, **77,** 603–621.

——, 1982: *Atmosphere–Ocean Dynamics.* Academic Press, 662 pp.

Godfrey, J. S., I. S. F. Jones, J. G. H. Maxwell and B. D. Scott, 1980: On the winter cascade from Bass Strait into the Tasman Sea. *Aust. J. Mar. Freshwater Res.*, **31,** 275–286.

Halpern, D., and J. R. Holbrook, 1972: STD measurements off the Oregon coast, July/August 1972. Coastal Upwelling Ecosystems Analysis, Data Rep. 4.

Hsieh, W. W., and A. E. Gill, 1984: The Rossby adjustment problem in a rotating, stratified channel, with and without topography. *J. Phys. Oceanogr.*, **14,** 424–436.

——, M. K. Davey and R. C. Wajsowicz, 1983: The free Kelvin wave in finite-difference numerical models. *J. Phys. Oceanogr.*, **13,** 1383–1397.

Holbrook, J. R., and D. Halpern, 1974: STD measurements off the Oregon coast, July/August 1973. Coastal Upwelling Ecosystems Analysis, Data Rep. 12.

LeBlond, P. H., and L. A. Mysak, 1978: *Waves in the Ocean.* Elsevier, 602 pp.

Mysak, L. A., 1980: Recent advances in shelf wave dynamics. *Rev. Geophys. Space Phys.*, **184,** 211–241.

——, C. Groot and K. Hamilton, 1986: A study of climate and fisheries: Interannual variability of the Northeast Pacific Ocean and its influence on homing migration routes of sockeye salmon. *Climatol. Bull.*, **20,** 26–35.

Ou, H. W., 1984: Geostrophic adjustment: A mechanism for frontogenesis. *J. Phys. Oceanogr.*, **14,** 994–1000.

Tomczak, M. Jr., 1985: The Bass Strait water cascade during winter 1981. *Contin. Shelf Res.*, **4,** 255–278.

Tully, J. P., 1942: Surface non-tidal currents in the approaches to Juan de Fuca strait. *J. Fish. Res. Bd. Can.*, **5,** 398–409.

Van Heijst, K. H., 1985: A geostrophic model of a tidal mixing front. *J. Phys. Oceanogr.*, **15,** 1182–1190.

Wang, D. P., 1984: Mutual intrusion of a gravity current and density front formation. *J. Phys. Oceanogr.*, **14,** 1191–1199.

Weaver, A. J., 1987: Bass Strait as a reverse estuary source for coastally trapped waves. *Aust. J. Mar. Freshwater Res.*, **38,** in press.